

3

AD-A167 715

NAVAL POSTGRADUATE SCHOOL

Monterey, California



DTIC
ELECTE
MAY 21 1986
S D

THESIS

THE VARIATION OF THE DISLOCATION DENSITY
IN ALUMINUM DEFORMED TO LARGE
STEADY-STATE CREEP STRAINS

by

T. Scott Wetter

March 1986

Thesis Advisor:

M. E. Kassner

Approved for public release; distribution is unlimited

86 5 21 124

DTIC FILE COPY

UNCLASSIFIED

SECURITY CLASSIFICATION OF THIS PAGE

REPORT DOCUMENTATION PAGE

1a. REPORT SECURITY CLASSIFICATION UNCLASSIFIED			1b. RESTRICTIVE MARKINGS		
2a. SECURITY CLASSIFICATION AUTHORITY			3. DISTRIBUTION/AVAILABILITY OF REPORT Approved for public release; distribution is unlimited		
2b. DECLASSIFICATION/DOWNGRADING SCHEDULE			4. PERFORMING ORGANIZATION REPORT NUMBER(S)		
4. PERFORMING ORGANIZATION REPORT NUMBER(S)			5. MONITORING ORGANIZATION REPORT NUMBER(S)		
6a. NAME OF PERFORMING ORGANIZATION Naval Postgraduate School		6b. OFFICE SYMBOL (if applicable) Code 69		7a. NAME OF MONITORING ORGANIZATION Naval Postgraduate School	
6c. ADDRESS (City, State, and ZIP Code) Monterey, California 93943-5100			7b. ADDRESS (City, State, and ZIP Code) Monterey, California 93943-5100		
8a. NAME OF FUNDING/SPONSORING ORGANIZATION		8b. OFFICE SYMBOL (if applicable)		9. PROCUREMENT INSTRUMENT IDENTIFICATION NUMBER	
8c. ADDRESS (City, State, and ZIP Code)			10. SOURCE OF FUNDING NUMBERS		
			PROGRAM ELEMENT NO.	PROJECT NO.	TASK NO.
			WORK UNIT ACCESSION NO.		
11. TITLE (Include Security Classification) THE VARIATION OF THE DISLOCATION DENSITY IN ALUMINUM DEFORMED TO LARGE STEADY-STATE CREEP STRAINS					
12. PERSONAL AUTHOR(S) Wetter, Timothy Scott					
13a. TYPE OF REPORT Master's Thesis		13b. TIME COVERED FROM TO		14. DATE OF REPORT (Year, Month, Day) 1986 March	
15. PAGE COUNT 56					
16. SUPPLEMENTARY NOTATION					
17. COSATI CODES			18. SUBJECT TERMS (Continue on reverse if necessary and identify by block number)		
FIELD	GROUP	SUB-GROUP	Superplasticity, Aluminum, Creep, Torsion testing, Subgrain size, Dislocation density		
19. ABSTRACT (Continue on reverse if necessary and identify by block number) This thesis reports trends in the variation of the subgrain size and density of dislocations not associated with subgrain boundaries (forest dislocations) in high purity aluminum with strain during primary and steady-state creep at temperatures in the power-law regime utilizing torsional deformation. Any microstructural feature responsible for strength is expected to be constant during steady-state deformation. Earlier work addressed changes in the subgrain size over a wide range of steady-state strain. A constant subgrain size was found. The present effort primarily examined					
20. DISTRIBUTION/AVAILABILITY OF ABSTRACT <input checked="" type="checkbox"/> UNCLASSIFIED/UNLIMITED <input type="checkbox"/> SAME AS RPT <input type="checkbox"/> DTIC USERS			21. ABSTRACT SECURITY CLASSIFICATION UNCLASSIFIED		
22a. NAME OF RESPONSIBLE INDIVIDUAL M. E. Kassner			22b. TELEPHONE (Include Area Code) 646-3036		22c. OFFICE SYMBOL

CONTINUED

UNCLASSIFIED

SECURITY CLASSIFICATION OF THIS PAGE (When Data Entered)

the dislocation density but also further evaluated the conclusion of a constant subgrain size during steady-state. The subgrain size data were found consistent with the earlier work. In contrast to constant-stress tests in other investigations, it was found, here, that the forest dislocation density monotonically increased until a steady-state at a strain of approximately 0.20. The forest dislocation density is essentially constant at steady-state. These two findings are consistent with dislocation network theories for creep. Optical micrographs were taken from tangential sections of the torsioned samples, which substantiated the finding that the subgrain size is fixed during steady-state. Keywords: Superplasticity

100-1000-1000-1000

UNCLASSIFIED

SECURITY CLASSIFICATION OF THIS PAGE (When Data Entered)

Approved for public release; distribution is unlimited.

The Variation of the Dislocation Density in Aluminum
Deformed to Large Steady-State Creep Strains

by

T. Scott Wetter
Lieutenant, United States Navy
B.A., University of Illinois, 1977

Submitted in partial fulfillment of the
requirements for the degree of

MASTER OF SCIENCE IN MECHANICAL ENGINEERING

from the

NAVAL POSTGRADUATE SCHOOL
March 1986

Author:


T. Scott Wetter

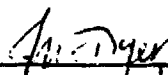
Approved by:



M. E. Kassner, Thesis Advisor



Paul J. Marro, Chairman,
Department of Mechanical Engineering



John N. Dyer,
Dean of Science and Engineering

ABSTRACT

This thesis reports trends in the variation of the subgrain size and density of dislocations not associated with subgrain boundaries (forest dislocations) in high purity aluminum with strain during primary and steady-state creep at temperatures in the power-law regime utilizing torsional deformation. Any microstructural feature responsible for strength is expected to be constant during steady-state deformation. Earlier work addressed changes in the subgrain size over a wide range of steady-state strain. A constant subgrain size was found. The present effort primarily examined the dislocation density but also further evaluated the conclusion of a constant subgrain size during steady-state. The subgrain size data were found consistent with the earlier work. In contrast to constant-stress tests in other investigations, it was found, here, that the forest dislocation density monotonically increased until a steady-state at approximately $\epsilon = 0.20$. The forest dislocation density is essentially constant at steady-state. These two findings are consistent with dislocation network theories for creep. Optical micrographs were taken from tangential sections of the torsion samples, which substantiated the finding that the subgrain size is fixed during steady-state.

TABLE OF CONTENTS

I.	INTRODUCTION	8
	A. RESEARCH IMPORTANCE	8
II.	BACKGROUND	10
	A. THEORY	10
	B. BACKGROUND	12
III.	EXPERIMENTAL PROCEDURES	18
	A. SPECIMEN TESTING	18
	B. TEM SAMPLE PREPARATION	19
	C. TENSILE TEST	20
	D. SUBGRAIN OPTICAL MICROSCOPY	20
	E. DATA REDUCTION	21
IV.	RESULTS AND DISCUSSION	26
V.	CONCLUSIONS AND RECOMMENDATIONS	36
	APPENDIX A: SUBGRAIN DATA	37
	APPENDIX B: DISLOCATION DATA	40
	LIST OF REFERENCES	53
	INITIAL DISTRIBUTION LIST	55

Accession For	
NTIS CRA&I	<input checked="" type="checkbox"/>
DTIC TAB	<input type="checkbox"/>
Unannounced	<input type="checkbox"/>
Justification	
By _____	
Distribution /	
Availability Codes	
Dist	Avail and/or Special
A-1	



LIST OF TABLES

I	COMPARATIVE DISLOCATION DENSITY AND SUBGRAIN SIZE DATA	33
---	---	----

LIST OF FIGURES

2.1	Typical elevated-temperature stress versus strain behavior of a pure metal deformed at a constant strain-rate [Ref. 1]	16
2.2	Comparison of a deformed and undeformed torsion specimen	17
2.3	Torsional deformation of Type 304 stainless steel at $T = 1138 \text{ K}$ and $\dot{\epsilon} = 3.32 \times 10^{-5} \text{ s}^{-1}$ [Ref. 10]	18
3.1	Standard dimensions in inches of the torsion specimens used in this investigation [Ref. 1]	27
3.2	Illustration of sectioning of the torsion specimen for TEM thin-foil preparation	28
4.1	Tension and torsion test plot	34
4.2	TEM micrographs of Al deformed to strains of 0.60 and 7.89	35
4.3	Subgrain size verses true strain (a) a strain range of 0 to 0.65 and (b) 0 to 16.33. ($\lambda_{ave_{ss}} \cong 12.73 \text{ microns}$)	36
4.4	Optical micrographs of tangential sections of Al deformed to strains of 0.20 and 14.3	37
4.5	TEM micrograph of the dislocations not associated with subgrains in an Al specimen deformed to a strain of 6.33	38
4.6	Dislocation density versus true strain (a) strain range of 0 to 0.65 and (b) 0 to 16.33. ($\rho_{ave_{ss}} \cong 1.39 \times 10^{12}/\text{m}^2$)	39

I. INTRODUCTION

A. RESEARCH IMPORTANCE

The strength (hardening) of materials subject to high temperatures is a critical concern in industry and science. As increasing commercial pressure is created by diminishing natural resources, greater efficiency is being demanded from machinery. This creates an increased need to better predict the behavior of the material. This research seeks to isolate the specific cause of strengthening of aluminum under such high temperature conditions. This will help the technical community to develop microstructurally based constitutive equations.

This work is part of a larger study to determine the details of the high temperature strength in metals and resolve the controversy over the relative hardening contributions of dislocation density (ρ), subgrain size (λ) and subgrain misorientation angle (θ). Aluminum (99.999% purity) was selected for this work because of its very high ductility. The combination of high ductility and the use of torsion testing versus tension testing allowed investigation of the dislocation microstructure (λ and ρ) well into steady-state. The testing temperature and strain-rate corresponded to the power-law creep regime. An earlier study [Ref. 1] developed foil preparation techniques and observed the subgrain size versus strain trends. This thesis expanded the earlier study to include more λ versus strain data as well as the forest dislocation density versus strain data. A subsequent study will examine the subgrain misorientation angle (θ) versus primary and steady-state strain.

During steady-state, the temperature, strain-rate and flow stress are constant and the microstructural feature associated with the rate-controlling process of creep should be fixed. Therefore, by following the λ and ρ versus strain trends, insight into the microstructural feature associated with creep strength could be identified. This is an important first step in developing equations that could predict strength on the basis of such fundamental variables as temperature, strain-rate, and defect microstructure.

II. BACKGROUND

A. THEORY

When pure metals are deformed at elevated temperatures, we observe strain hardening. However, with this hardening there is a parallel softening or recovery and with strain, a steady-state condition is attained and the flow stress is constant (see Fig. 2-1) in a constant strain-rate test.

Strain hardening (strengthening) in metals at elevated temperatures ($T > 0.6T_m$) in the power-law creep range is associated with the formation of dislocations as the strain increases. These dislocations form into two basic morphologies. First, random or forest dislocations are present. These dislocations can be described in terms of a forest dislocation density (ρ). Second, some of the dislocations form low energy configurations or subgrain boundaries. Several sets of dislocations each with its own Burgers vector comprise the subgrain boundaries which have a characteristic dislocation spacing (d) or misorientation angle (θ). There is a great deal of controversy over which of these features (subgrains or forest dislocations) are associated with the hardening or strength. Generally, the subgrain size λ is regarded as an obstacle spacing for gliding or mobile dislocations and d (or θ) is often regarded as the distance over which edge segments of mobile dislocations must climb and annihilate in order that subsequent plasticity within the subgrain continue. The spacing, d , may also affect the effectiveness of the grain boundary as an obstacle to dislocations and affect the ease of dislocation emission from the boundary.

It is believed that any source of material strengthening must be constant during steady-state since no net hardening is evident. To determine which microstructural feature

remains unchanged, a special test procedure can be used. In the present method, a constant strain-rate technique was used to identify features that might change with strain. Here, several torsion specimens were deformed to various primary but, principally, steady-state strains and quenched. Transmission electron microscopy was used to measure λ and ρ . ρ and λ were noted for any deviations. A change during steady-state implied independence from any strengthening mechanism.

Another method to discriminate between subgrain and forest dislocation strengthening is to emphasize transient rather than steady-state microstructures. That is, once steady-state has been achieved, either the stress (constant-stress creep test) or the strain-rate (constant strain-rate creep test) is changed. Eventually a new steady-state is achieved corresponding to the new creep conditions. The strain over which the new steady-state is achieved is termed transient creep. Some investigators observe the change in the microstructure during a transient creep test and attempt to isolate those features (λ , ρ or d) which best correlate with the creep-rate or creep stress.

However, it is believed that a disadvantage of stress reduction testing is that it may be ambiguous. Two difficulties may be (a) the inability to accurately measure low transient creep rates after a large stress reduction, and (b) the uncertainty of deciding which creep rate to use after stress reduction, since creep rate recovery is usually a complex interaction of elastic, anelastic and plastic deformation [Ref. 1].

At steady-state, there is always a strict relationship between λ_{ss} and ρ_{ss} as seen below:

$$\lambda_{ss} = K'(\sigma_{ss}/E)^{-1} \quad (\text{eqn 2.1})$$

where K' is a constant, σ_{ss} is steady-state stress and E is the Young's modulus. Also:

$$\rho_{ss} = K''(\sigma_{ss}/E) \quad (\text{eqn 2.2})$$

where ρ_{ss} is the steady-state forest dislocation density [Ref. 1].

Because both the subgrain size and forest dislocation density correlate with the steady-state stress, it is impossible to discriminate between the strengthening by these features in steady-state microstructures.

All of the tests in this research were performed in the power-law creep range. Here, the activation energy for creep is essentially that of self-diffusion of the metal, which is a known quantity. The following relationship is observed:

$$\dot{\epsilon}_{ss} = K''' \exp(-Q/RT)(\sigma_{ss}/E)^n \quad (\text{eqn 2.3})$$

where σ_{ss} is the steady-state stress, $\dot{\epsilon}_{ss}$ is the steady-state strain-rate and n is the steady-state strain-rate sensitivity exponent. In the power law range, $n \cong 5$ [Ref. 2].

B. BACKGROUND

Creep investigators can be grouped into two categories: those that believe that, in subgrain forming materials, the details of the subgrains (d or λ) control the creep strength and those that believe the forest or random dislocations are more important. The former group will be discussed first.

Ferreira and Stang used optical techniques on transient creep (stress-dip) tests [Ref. 2] and concluded that the strength is associated with subgrain size. Dislocations were not observed. Soliman, Ginter and Mohamed [Ref. 3], Young, Robinson and Sherby [Ref. 4] and Kikuchi and Yamaguchi [Ref. 5] used TEM techniques and stress reduction tests and also concluded subgrain strengthening. Again, dislocations were not considered [Ref. 1]. Calliard and Martin [Ref. 6] came to the same determination, this time including dislocation density data. Here, the dislocations were considered to be only weak obstacles to gliding dislocations [Ref. 1].

The second group believes that forest dislocations are the controlling factor in restricting the movement of gliding dislocations. Langdon, Vastava and Yavari [Ref. 7] used stress reduction techniques with the TEM, and concluded that forest dislocation strengthening dominated since the subgrain size remained constant despite changes in strain-rate. Parker and Wilshire [Ref. 8] had similar results [Ref. 1].

Kassner, Ziaai-Moayyed and Miller [Ref. 9] used 304 stainless steel and concluded that the forest dislocation density controlled strengthening [Ref. 1]. Kassner and Elmer [Ref. 10] observed the dependence of three microstructural features (ρ , λ , and the spacing of dislocations comprising the subgrain boundaries, d) with the transient and steady-state creep strain using torsional deformation. As shown in (Figure 2.3), during steady-state, where $\dot{\epsilon}$, σ and T are constant, λ changed while ρ was fixed. This suggested that ρ rather than λ controlled creep strength. Unfortunately, carbide precipitation and subsequent cavitation at the grain boundaries precluded deformation to strains greater than about one. For this reason the microstructural parameters versus steady-state strain trends were inconclusive [Ref. 1].

A recent thesis by Mieszczański [Ref. 1] used the same torsional techniques of [Ref. 10] on much more ductile aluminum. The results were incomplete since only subgrains were observed. This thesis expanded his work by examining ρ versus strain using the same thin-foils prepared in [Ref. 1] along with three new quenched torsion specimens to better define the trends. This research project, as well as that of [Ref. 1] examined the dislocation microstructure in specimens deformed up to strains of 16.33. This allows for a more definitive determination of both transient and especially steady-state trends in ρ and λ versus strain than in the previous work by Kassner and coworkers.

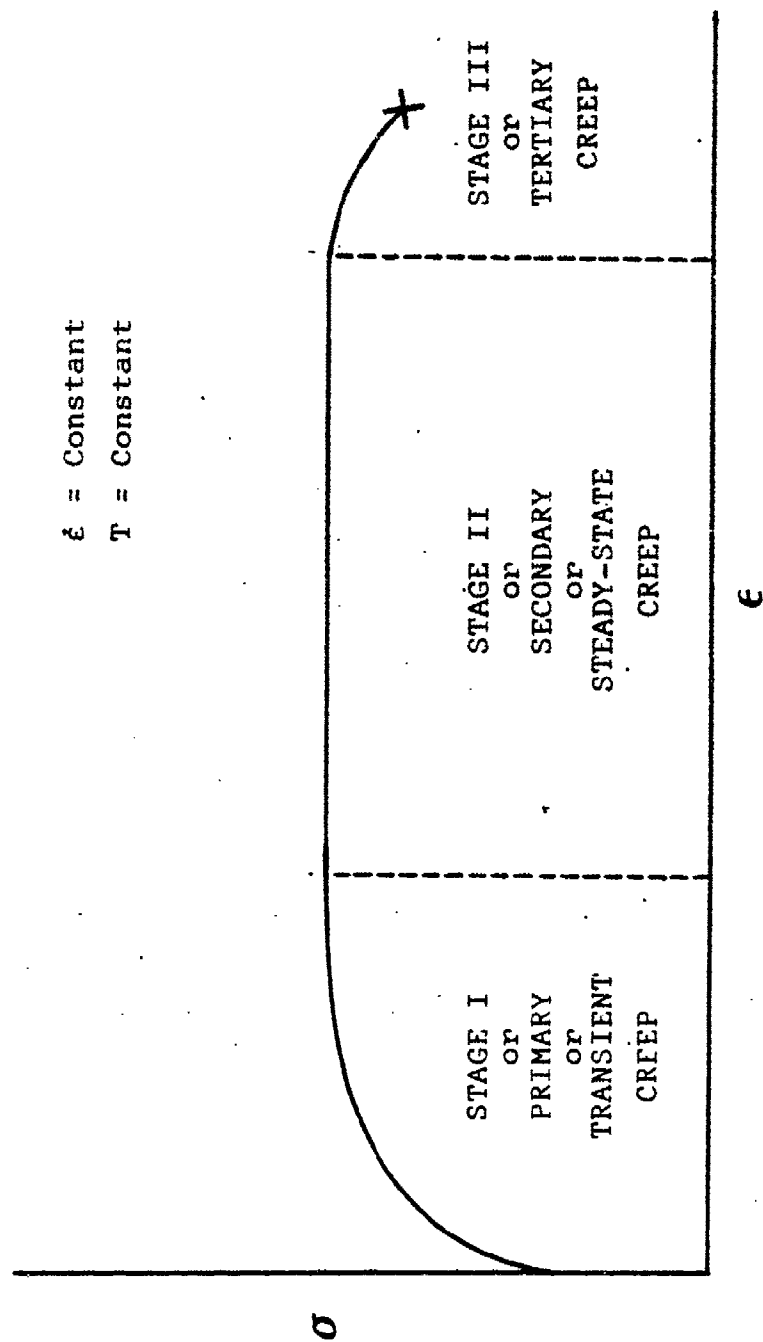


Figure 2.1: Typical elevated-temperature stress versus strain behavior of a pure metal or subgrain-forming alloy [Ref. 1].

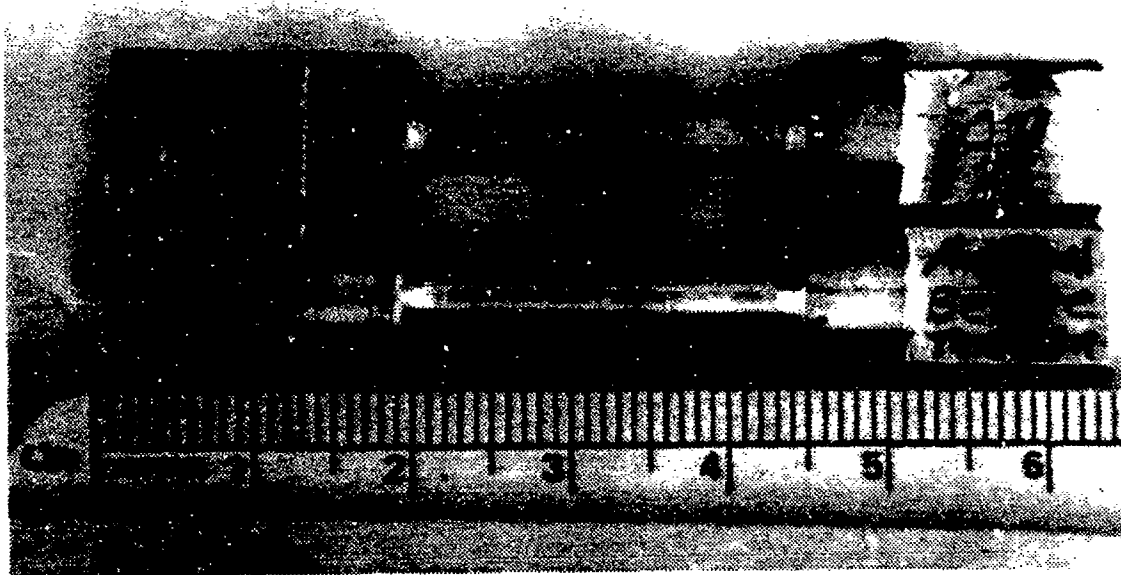


Figure 2.2 Comparison of a deformed and undeformed torsion specimen.

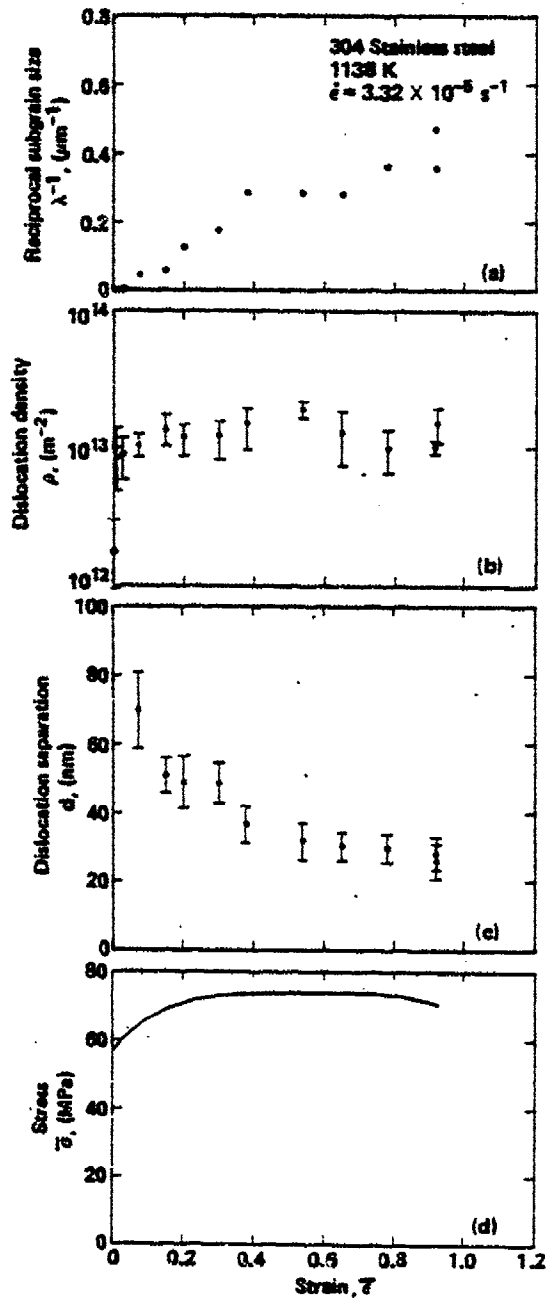


Figure 2.3: Torsional deformation of Type 304 stainless steel at $T = 1138 \text{ K}$ and $\dot{\epsilon} = 3.32 \times 10^{-5} \text{ s}^{-1}$. (a) reciprocal subgrain size, λ^{-1} , versus strain, ϵ ; (b) forest dislocation density, ρ , versus ϵ ; (c) subgrain boundary dislocation separation, d , versus ϵ ; (d) stress, σ , versus ϵ . [Ref. 10].

III. EXPERIMENTAL PROCEDURES

A. SPECIMEN TESTING

99.999% pure aluminum was used as stock for the torsion specimens. The material was supplied by the Materials Research Corporation as 5/8 inch diameter rod. The samples were machined to a gage section of 5.1 mm diameter and 25.4 mm length. The specimen dimensions are illustrated in (Fig. 3-1).

The specimens were annealed in a vacuum at 698 K for one hour. The samples were then twisted in a torsion machine at Stanford University in Stanford, California. The machine is powered by a ten horsepower electric motor which drives a reduction assembly comprised of two-four speed truck transmissions and two dual chain sprocket assemblies, all coupled in series. This assembly drives a specimen grip which is coupled to the assembly by an electromagnetic clutch. The clutch assembly allows specimen rotation only after the assembly reaches constant speed subsequent to start-up and also allows instantaneous rotation termination upon quenching. The second grip is stationary and connected to a torsional load cell. A quartz tube surrounds the specimen and grips. Through this quartz tube, high purity argon (99.999%) is passed during specimen heating and deformation. The quartz tube has a side arm which connects to a solenoid valve through which water under pressure may pass to provide a quench of the specimen immediately after high temperature deformation. The quench rate has been estimated at 1200 to 1800 degrees Kelvin per second. A dual elliptical furnace provides a rapid heating rate. Nickel foil was wrapped about the external circumference of the quartz tube to provide uniform heating of the specimen and minimize temperature variations within the sample as a function of time.

The specimen temperature was maintained within 3 degrees K. The specimen ends were coated with lubricant to reduce the possibility of tensile or compressive stresses in the specimen as a result of slight changes in specimen length during the course of the deformation.

The strain-rate and temperature were held constant at 5.04×10^{-4} per second and 644 K. Eleven torsion specimens were tested from a primary true equivalent-uniaxial creep strain of 0.03 to a strain of 16.33. Torsion testing avoids the necking encountered in tensile testing and, therefore, allows deformation to large strains. (Fig. 2-2) compares an undeformed and deformed ($\epsilon = 16.33$) torsion specimen.

B. TEM SAMPLE PREPARATION

The specimens were first sectioned transversely (perpendicular to the long axis of the specimen) using a South Bay Technology Model 650 Low Speed Diamond Wheel Saw and a high concentration Buehler (.006") wafering blade. Slabs of aluminum were next removed from the outer layer of the sectioned torsion cylinders by slicing parallel to the long axis. 3 mm discs were spark cut from these slabs (Fig. 3). The slabs were mounted using a conductive glue on copper trays. A Servomet type SMD spark machine (set at HT 5) using brass cutting tubes was used for the extraction. The spark cut disks were ground using 600 grit silicon carbide paper.

It was found however that grinding annealed Al disks to thicknesses less than 0.45 mm would cause mechanical damage in 3 to 4 mm grain size aluminum as manifested by an increase in dislocation density in the central volume of the material [Ref. 11]. Therefore the disks were ground to not less than 0.45 mm thickness. The disks were next electropolished to perforation. An electrolyte of 469 parts methyl alcohol, 25 parts sulfuric acid and 6 parts hydrofluoric acid was used at 248 K, 25 volts and 12

milliamps. A pump setting of 10 was used for 3 minutes, then the pump was lowered to 7.5. The samples were electropolished until perforation occurred. The foils were examined using a 200 KV JEOL JEM-200CX electron microscope using a double tilt stage located at Lawrence Livermore National Laboratory.

C. TENSILE TEST

An aluminum tensile specimen was manufactured from a torsion specimen. A 3/32 inch hole was centered in each flange section. The sample was sealed in quartz under a vacuum, then annealed at 698 K for one hour. It was furnace cooled to ambient temperature. A 0.75 inch long cylindrical piece of hardened steel was used to connect the flange surface to the Instron grips.

Next the sample was placed in an Instron tensile testing machine. Extreme care was taken to avoid preloading the specimen. Four temperature sensing points were used; the upper flange temperature, the upper gage section temperature, the lower gage section temperature and the lower flange temperature. All four thermocouples were wired to a potentiometer.

An Omega three coil heating unit with extra insulation was placed around the test assembly. The temperature was held constant (once all four thermocouples indicated 644 K) for twenty minutes to ensure stability. The Instron utilized a strain rate of 3.33×10^{-4} per second (a cross-head speed of 0.02 inches per minute), a chart speed of 2 inches per minute and a full scale load range of 100 lbs.

D. SUBGRAIN OPTICAL MICROSCOPY

Tangential sections, as in (Fig. 3.2) of all 11 samples were polished to allow optical pictures to be taken of the deformed specimens. The specimens were first ground using 180 grit silicon carbide paper. The tangential section

included the undeformed grip, the tapered gage shoulder and the gage section. The samples were hand ground through successively finer silicon carbide paper through 600 grit. They were next polished on 6 micron and, finally, 1 micron diamond polishing wheels. The samples were then electropolished for 10 minutes in a 80% methanol, 20% nitric acid solution held at 253 K, 15 volts and 12 mA. This was followed by a 2 minute anodizing treatment using 92% water, 8% fluoboric acid at room temperature and 20 volts. The specimens were examined and photographed using a MAGOMET ECHO 3 machine located at Lawrence Livermore National Laboratory.

E. DATA REDUCTION

The data reduction procedures used in the torsion analysis and subgrain size analysis are the same as those used in [Ref. 1] and are repeated here for completeness.

Torsional Analysis

Equivalent uniaxial stress and strain values were converted from torque, and angle of twist measurements using the following relations [Ref. 1]:

$$\gamma = \alpha R/L \quad (\text{eqn 3.1})$$

where, γ = shear strain at the full radius position

α = angle of twist

R = radial distance to the outer fiber

L = gage length

$$\tau = M(3+n+m)/2\pi R^3 \quad (\text{eqn 3.2})$$

where, τ = surface shear stress

M = applied twisting moment

n = strain hardening exponent ($n=0$ at steady state)

m = strain-rate sensitivity exponent (approximately 0.13 at $\dot{\epsilon} = 0$ and 0.2 at steady-state)

$$\sigma = \sqrt{3}\tau \quad (\text{eqn 3.3})$$

where, σ = equivalent uniaxial stress, and

$$\epsilon = \gamma/\sqrt{3} \quad (\text{eqn 3.4})$$

where, ϵ = equivalent uniaxial strain (the von Mises criterion).

Subgrain Size Analysis

The average subgrain size was estimated by placing over several transmission electron microscope micrographs (usually 20) random test lines of a total length, L . The number of intersections between the lines and subgrain boundaries N_L allow an estimation of the subgrain size by:

$$\lambda = L/(N_L M) \quad (\text{eqn 3.5})$$

where, λ = average subgrain size

M = negative magnification

N_L = number of subgrain boundary intersections

L = length of random test lines (350 mm per

micrograph)

Dislocation Density Analysis

The average density of dislocations not associated with subgrain boundaries was calculated by the surface intersection technique of Ham and Sharpe [Ref. 12]. It is believed that in pure aluminum, dislocations might escape from the thin foil, and that the number may be a function of foil thickness [Ref. 13]. For this reason, dislocation density determinations were performed in thicker portions of the foil. The thickness of the foil at the photographic site was always between 12 and 15 $\langle 111 \rangle$ extinction distances (approximately $1\mu\text{m}$). It is known that $1/6$ of the dislocations are not visible (i.e. $g \cdot b = 0$) when viewed with a $\langle 220 \rangle$ g vector [Ref. 13]. No correction was made to the data on the basis of this consideration. The density was determined by counting the number of dislocations in 20 micrographs taken from the foils extracted from each specimen. The following equation was utilized:

$$\rho = N(M)^2/A \quad (\text{eqn 3.6})$$

where, ρ = density in dislocations per square meter
N = number of dislocations viewed in the slide
M = negative magnification
A = area of plate in square meters

Dislocations that comprise subgrains as well as dislocations that belonged to ambiguous features, i.e. tangles that may have a degree of perfection less than subgrain boundaries but greater than cell walls, were not included in the ρ calculations.

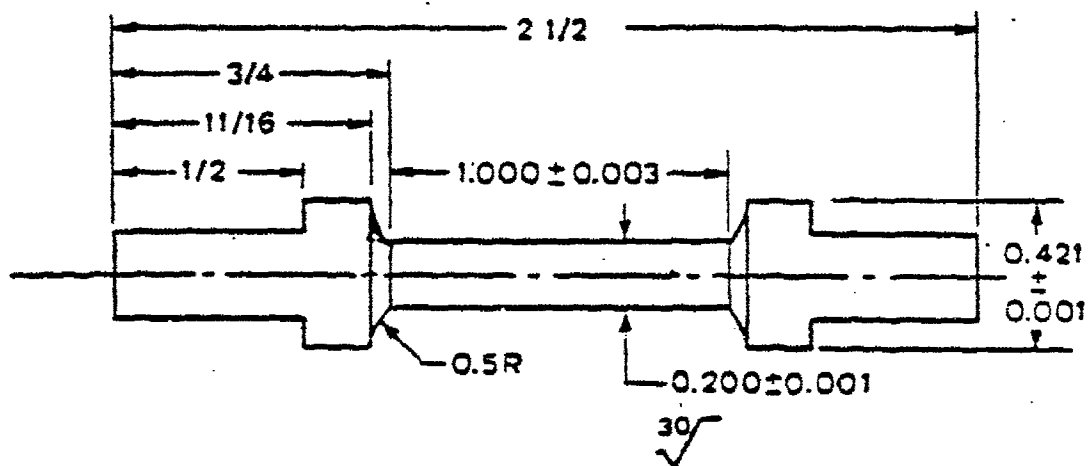


Figure 3.1: Standard dimensions in inches of the torsion specimens used in this investigation [Ref. 1].

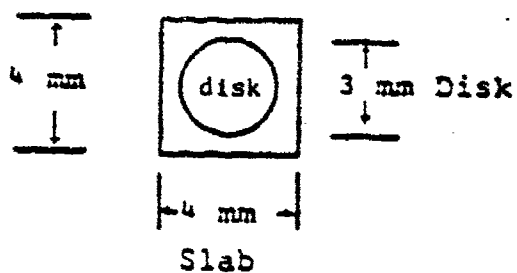
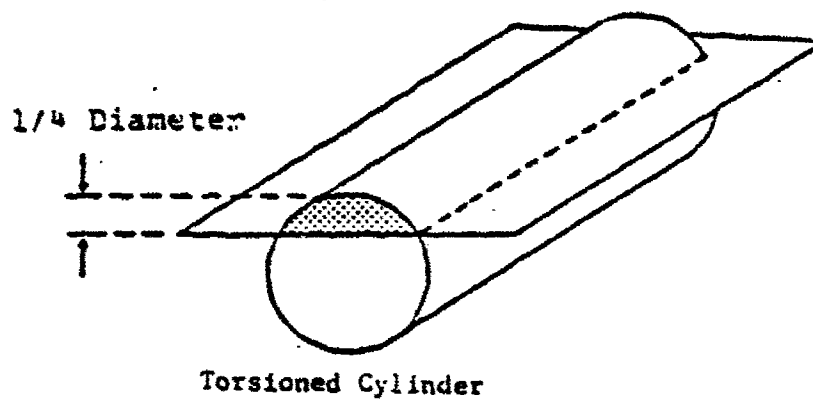


Figure 3.2 Illustration of sectioning of the torsion specimen for TEM thin-foil preparation.

IV. RESULTS AND DISCUSSION

Four new mechanical tests were performed in this research. One specimen was tested in tension using the Instron tensile testing machine at 644 K and an $\dot{\epsilon}$ of 3.33×10^{-4} per second. Fig. 4-1 shows that prior to the onset of necking at a true strain of 0.15, the data correlated reasonably well with the observed torsion tests. Three more torsion specimens were analyzed for subgrain size and forest dislocation density after being tested to strains of 0.03, 0.20 and 6.33. Fig. 4-2 shows sample subgrain micrographs. The λ data is complimentary to the eight samples torsion tested in [Ref. 1] and the values are listed in Table I. The comparative results are plotted in (Fig. 4-3).

As anticipated, at very low strains ($\epsilon < 0.20$), few subgrains are apparent giving a very large average subgrain size. This size steadily decreased until a steady-state was reached at a strain of around 0.2. The subgrain size in the specimens deformed to strains of 0.20 and 6.33 were 11.27 microns and 13.73 microns respectively. They are consistent with the trends of [Ref. 1] which show that λ is essentially constant ($\lambda_{ave_{ss}} = 12.73$ microns) over a very wide range of steady-state strain. Appendix A lists the raw data.

(Fig. 4-3) shows optical micrographs taken at around 75x. One picture is from a specimen deformed to $\epsilon = 0.20$ and the other to $\epsilon = 16.33$. The subgrain sizes appear to be identical, although the definition is more pronounced at the higher strain.

Forest dislocation density data were taken from a total of 11 specimens: 3 from this study and 8 values were taken from unpolished disks prepared in [Ref. 1]. Typical TEM dislocation micrographs are shown in (Fig. 4-4). All micro-

graphs were taken at random and an effort was made to avoid any ambiguity associated with developing subgrain boundaries.

(Fig. 4-5) depicts the trend of forest dislocation density with strain. Points with strains less than 1 are reproduced on a separate graph to provide clarity in the primary creep region. The data is listed in Table I. The data point A-7, corresponding to a strain of 7.89, had an unexpectedly high dislocation density that may be indicative of foil preparation damage. Over steady-state the dislocation density appears to be constant and the average density is about $1.39 \times 10^{12}/\text{m}^2$. The value appears to be consistent with other creep work. Orlova, Tobolova and Cadek [Ref. 12] observed density values of about $2 \times 10^{12}/\text{m}^2$ in Al creep tested to steady-state at an identical stress and at a temperature of 573 K. Although there has been an abundance of aluminum creep investigations, only a few determined the variation of the forest dislocations with primary creep strain. Blum, Absenger and Feihauer [Ref. 14] and Morris and Martin [Ref. 15] performed constant stress creep tests on Al-11Zn. This alloy has creep properties that have been demonstrated to be essentially identical to pure Al, but is believed [Ref. 14] to have the advantage of preventing dislocation escape from the foil by the precipitation of zinc at dislocations when the creep specimen is cooled from the testing temperature. These two investigations found that during primary creep, ρ increases to a maximum value and then decreases. One study [Ref. 14] found a subsequent decrease to a steady-state value while the other [Ref. 15] noted the decrease to persist during steady-state. This study, which utilized constant strain-rate tests, found a monotonic increase in the dislocations to steady-state. The former observation might be interpreted as evidence that forest dislocations do not provide strength since ρ is

observed to decrease during primary creep where the material experiences hardening. However, another explanation might be a high initial mobile dislocation density associated with relatively high initial creep-rates during primary creep as predicted by the equation:

$$\dot{\epsilon} = \rho_m v b / 2$$

(eqn 4.1)

where b is the Burgers vector, v the mobile dislocation velocity and ρ_m the mobile dislocation density. The high initial strain-rates give a high ρ_m and perhaps a high total dislocation density measured by ρ .

In the present tests, the strain-rate is constant and ρ_m may be constant. Hence, the observation of an increasing ρ during primary creep may imply that ρ is associated with hardening. When steady-state is achieved, ρ is constant.

There are available creep theories that associate creep strength with the forest dislocation theories. McLean [Ref. 16] proposed an early dislocation network theory. Later investigators [Ref. 17-18] provided some modification to this theory. Basically, network theories consider the forest dislocations a three-dimensional network within the subgrains. The nature of transient of steady-state creep is explained by network coarsening (diffusion controlled) and glide multiplication of dislocations.

TABLE I
COMPARATIVE DISLOCATION DENSITY AND SUBGRAIN SIZE DATA

SPECIMEN	TRUE STRAIN	DISLOCATION DENSITY ($10^{12}/\text{m}^2$)	SUBGRAIN SIZE (MICRONS)
A - 13	0.03	1.03	44.07
A - 6	0.10	1.32	15.35
A - 12	0.20	1.12	11.27
A - 3	0.60	1.08	10.57
A - 4	1.26	2.08	12.60
A - 1	3.11	1.15	13.80
A - 5	4.05	1.09	12.30
A - 11	6.33	1.34	13.73
A - 7	7.89	4.24	15.92
A - 8	14.3	1.82	10.98
A - 9	16.33	1.86	13.47

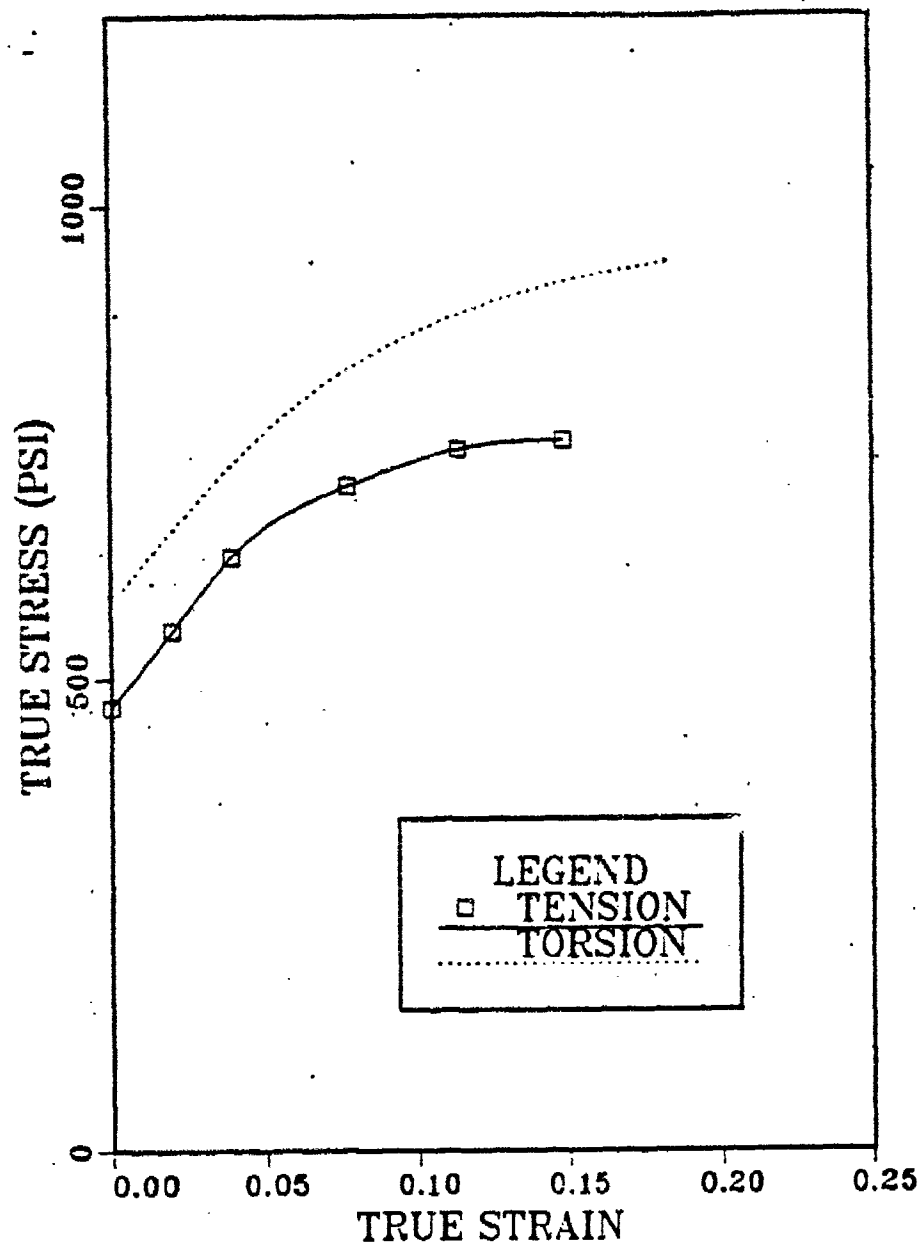
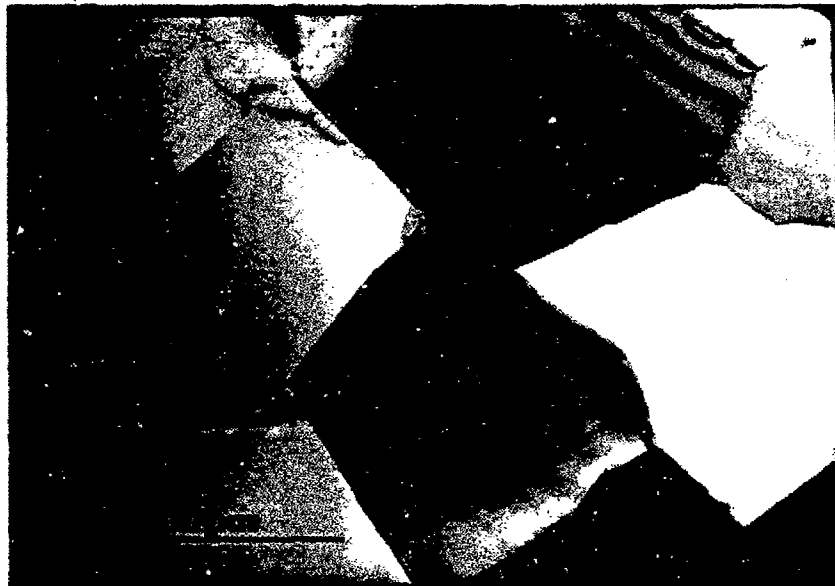


Figure 4.1 Tension and torsion test plot.



$\epsilon = 0.60$



$\epsilon = 7.89$

Figure 4.2 TEM micrographs of Al deformed to strains of 0.60 and 7.89.

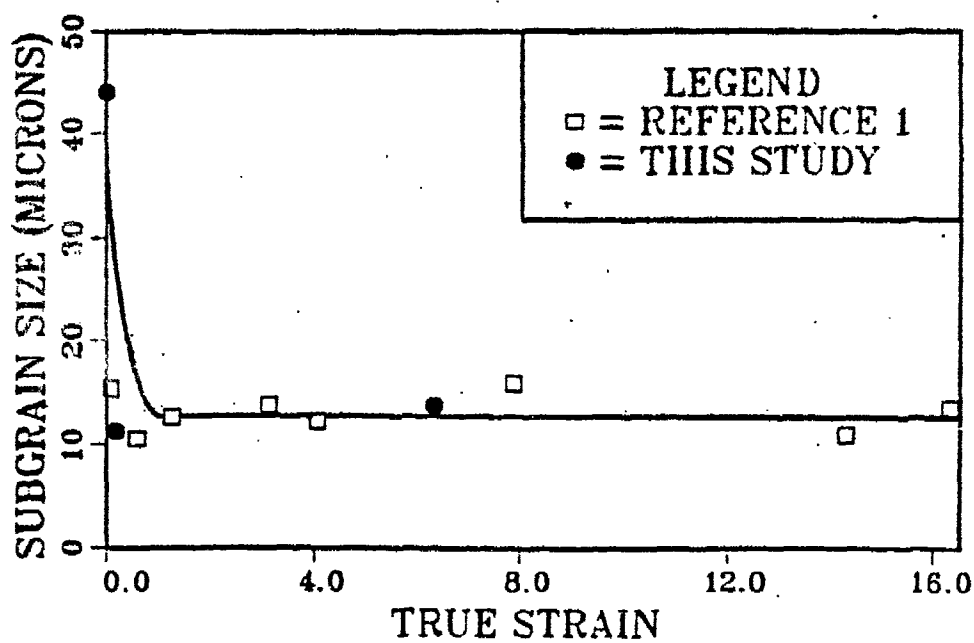
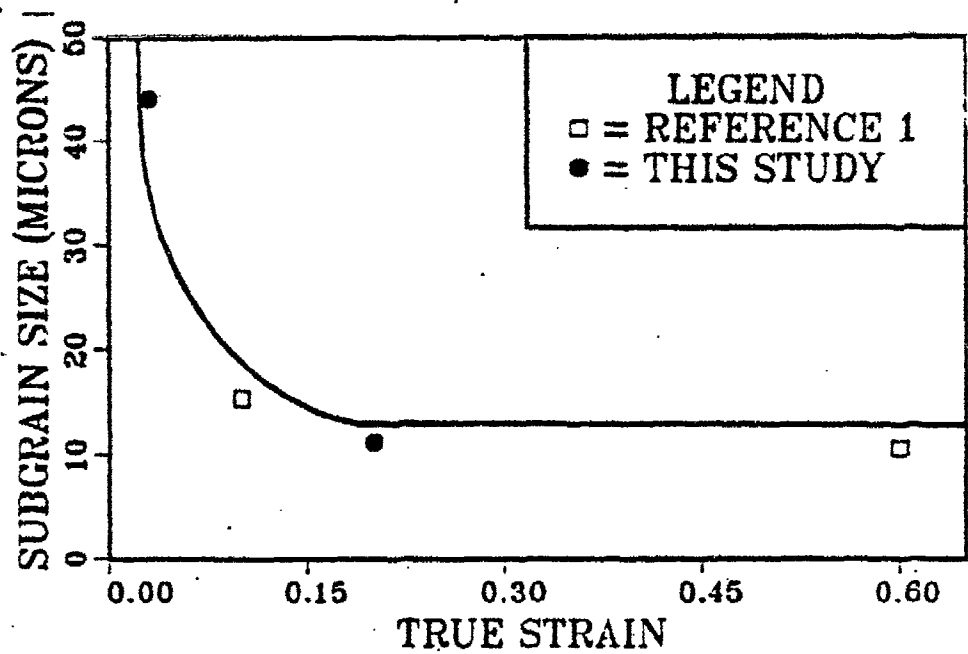
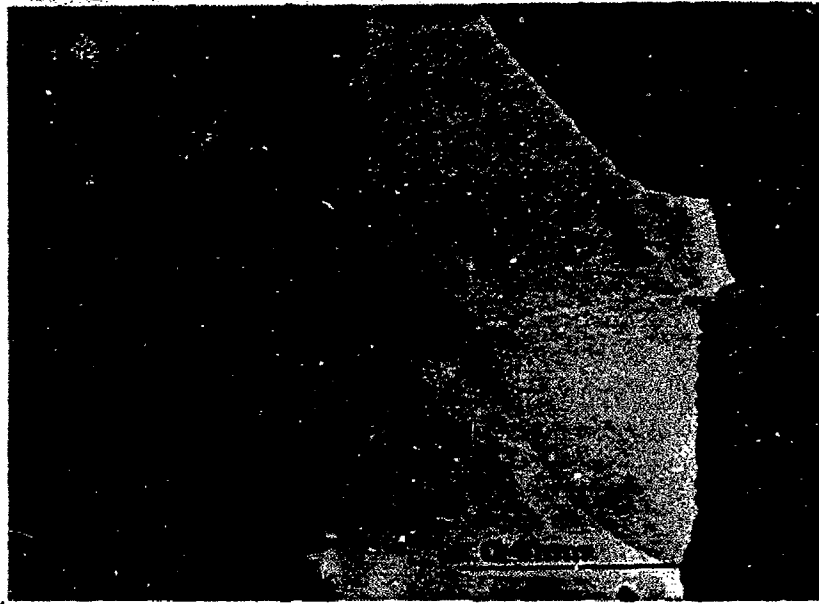
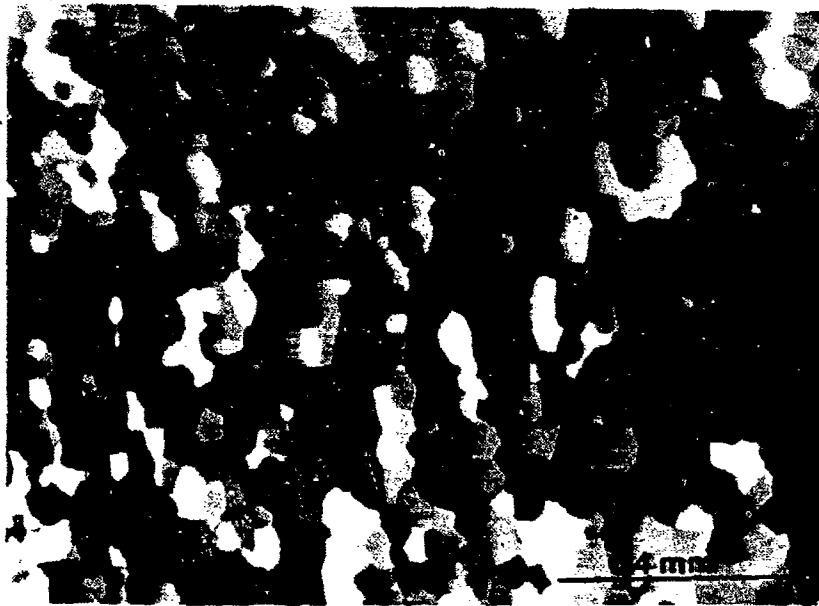


Figure 4.3 Subgrain size verses true strain
 (a) a strain range of 0 to 0.65 and (b) 0 to 16.33.
 ($\lambda_{ave_{ss}} \cong 12.73$ microns).



$\epsilon = 0.20$



$\epsilon = 14.3$

Figure 4.4 Optical micrographs of tangential sections of Al deformed to strains of 0.20 and 14.3.

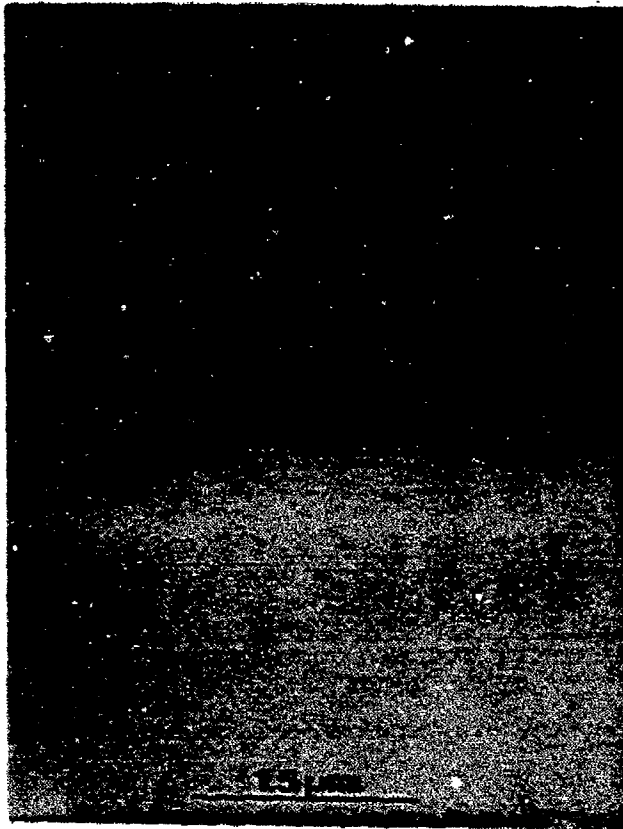


Figure 4.5 TEM micrograph of the dislocations not associated with subgrains in an Al specimen deformed to a strain of 6.33.

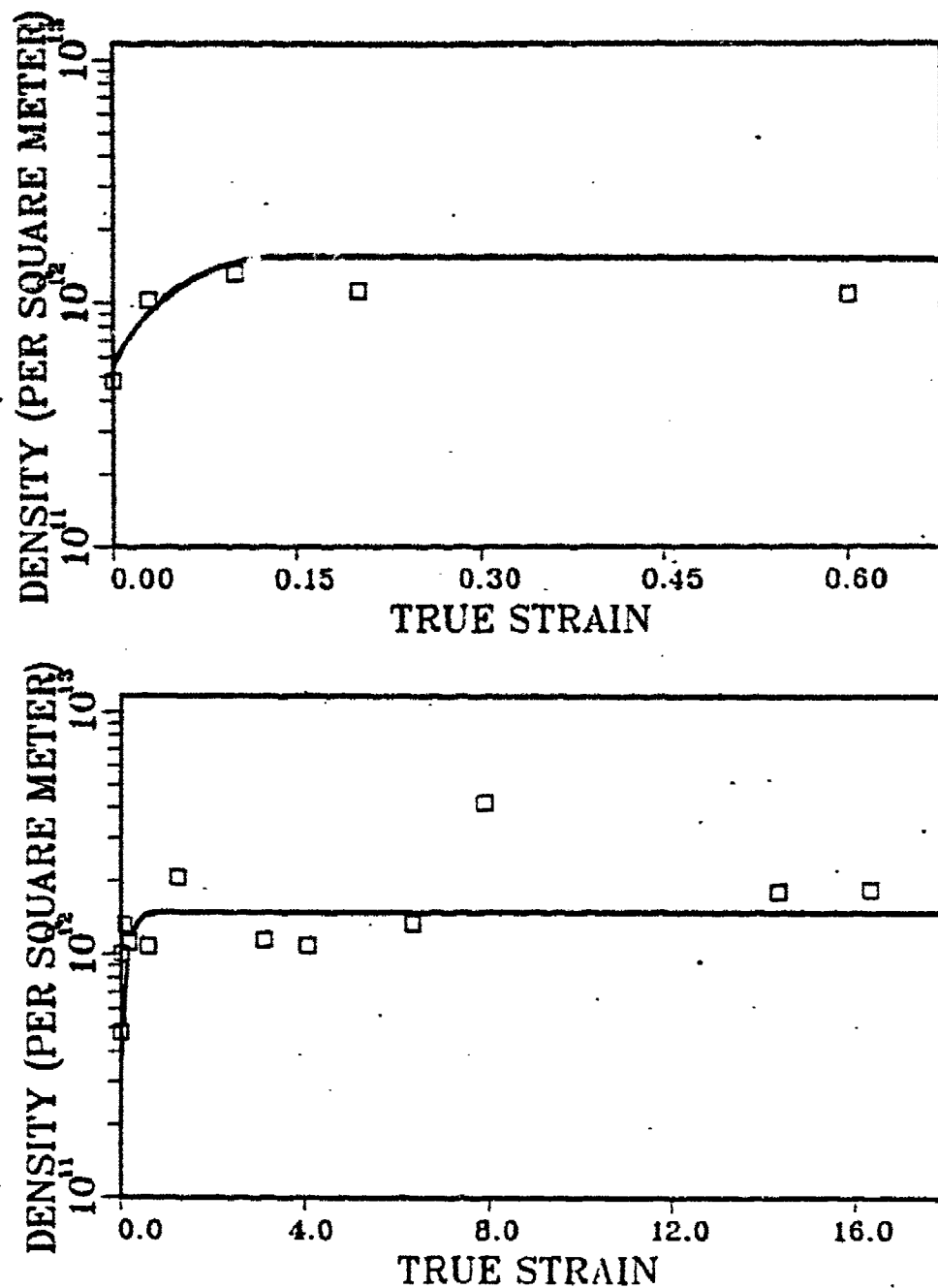


Figure 4.6 Dislocation density versus true strain
 (a) strain range of 0 to 0.65 and (b) 0 to 16.33.
 ($\rho_{ave_{ss}} \approx 1.39 \times 10^{12}/m^2$).

V. CONCLUSIONS AND RECOMMENDATIONS

This research on the dislocation microstructure of aluminum undergoing primary and steady-state creep has produced the following conclusions:

1. The subgrain size remained essentially constant once steady-state had been reached.
2. It was also found that the forest dislocation density is approximately constant during steady-state.
3. Contrary to earlier conclusions based on constant-stress creep-tests, no peak forest dislocation density was observed prior to reaching steady-state. The density increased monotonically to steady-state.
4. These results, though not conclusive, provide somewhat more support for the dislocation network theory of creep which suggests that the forest dislocation density controls the creep strength.

APPENDIX A
SUBGRAIN DATA

TABLE A.1

Specimen A-11, $\epsilon = 6.33$, $T = 644K$, $\dot{\epsilon} = 5.04 \times 10^{-4} s^{-1}$

$\lambda_{ave} = 13.73 \mu m$

<u>Foil No.</u>	<u>Micrograph No.</u>	<u>Magnification</u>	<u>No. Intercepts for 350 mm of random lines</u>
A-11,3	8736	3000x	7
A-11,3	8737	3000x	7
A-11,3	8738	3000x	7
A-11,3	8739	3000x	6
A-11,3	8740	3000x	10
A-11,3	8741	3000x	8
A-11,3	8742	3000x	13
A-11,3	8743	3000x	11
A-11,3	8744	3000x	5
A-11,3	8745	3000x	9
A-11,3	8746	3000x	5
A-11,3	8747	3000x	11
A-11,4	8760	3000x	6
A-11,4	8761	3000x	11
A-11,4	8762	3000x	3
A-11,4	8763	3000x	9
A-11,4	8764	3000x	8
A-11,4	8765	3000x	15
A-11,4	8766	3000x	10
A-11,4	8767	3000x	8
A-11,4	8768	3000x	7
A-11,4	8769	3000x	13
A-11,4	8770	3000x	6
A-11,4	8771	3000x	9

TABLE A.2

Specimen A-12, $\varepsilon = 0.20$, $T = 644\text{K}$, $\dot{\varepsilon} = 5.04 \times 10^{-4} \text{s}^{-1}$ $\lambda_{\text{ave}} = 10.35 \mu\text{m}$

<u>Foil No.</u>	<u>Micrograph No.</u>	<u>Magnification</u>	No. Intercepts
			for 350 mm of <u>random lines</u>
A-12,1	8562	3000x	10
A-12,1	8563	3000x	13
A-12,1	8564	3000x	14
A-12,1	8565	3000x	7
A-12,1	8566	3000x	10
A-12,2	8551	3000x	11
A-12,2	8552	3000x	16
A-12,2	8553	3000x	10
A-12,2	8554	3000x	11
A-12,2	8555	3000x	6
A-12,2	8556	3000x	10
A-12,2	8557	3000x	7
A-12,2	8558	3000x	11
A-12,2	8559	3000x	7
A-12,2	8560	3000x	15
A-12,2	8561	3000x	13
A-12,2	8587	3000x	11
A-12,2	8588	3000x	5
A-12,2	8589	3000x	10
A-12,2	8590	3000x	10

TABLE A.3

Specimen A-13, $g = 0.03$, $T = 644\text{K}$, $\dot{\epsilon} = 5.04 \times 10^{-4} \text{s}^{-1}$ $\lambda_{\text{ave}} = 2.60 \mu\text{m}$

<u>Foil No.</u>	<u>Micrograph No.</u>	<u>Magnification</u>	<u>No. Intercepts for 350 mm of random lines</u>
A-13,2	8519	3000x	6
A-13,2	8520	3000x	1
A-13,2	8521	3000x	3
A-13,2	8522	3000x	0
A-13,2	8523	3000x	4
A-13,2	8524	3000x	4
A-13,2	8525	3000x	2
A-13,2	8526	3000x	3
A-13,2	8527	3000x	0
A-13,2	8528	3000x	3
A-13,2	8529	3000x	6
A-13,2	8530	3000x	3
A-13,2	8541	3000x	4
A-13,2	8542	3000x	2
A-13,2	8543	3000x	1
A-13,2	8544	3000x	3
A-13,2	8745	3000x	0

APPENDIX B
DISLOCATION DATA

TABLE B.1

Specimen A-1, $\epsilon = 3.11$, $\dot{\epsilon} = 5.04 \times 10^{-4} \text{ s}^{-1}$

$T = 644 \text{ K}$, $\lambda_{\text{ave}} = 13.80 \text{ } \mu\text{m}$

$\rho_{\text{ave}} = 1.15 \times 10^{12} / \text{m}^2$

<u>Foil No.</u>	<u>Micrograph No.</u>	<u>Magnification</u>	<u>Dislocations</u>
A-1,10	8438	20,000x	8
A-1,10	8439	20,000x	14
A-1,10	8440	20,000x	8
A-1,10	8441	20,000x	25
A-1,10	8442	20,000x	42
A-1,10	8443	20,000x	22
A-1,10	8444	20,000x	5
A-1,10	8445	20,000x	23
A-1,10	8446	20,000x	9
A-1,10	8447	20,000x	14
A-1,11	8448	20,000x	16
A-1,11	8449	20,000x	9
A-1,11	8450	20,000x	18
A-1,11	8451	20,000x	14
A-1,11	8452	20,000x	18
A-1,11	8453	20,000x	21
A-1,11	8454	20,000x	37
A-1,11	8455	20,000x	29
A-1,11	8456	20,000x	19
A-1,11	8457	20,000x	29

TABLE B.2

Specimen A-3, $\epsilon = 0.60$, $\dot{\epsilon} = 5.04 \times 10^{-4} \text{ s}^{-1}$ $T = 644 \text{ K}$, $\lambda_{\text{ave}} = 10.57 \text{ } \mu\text{m}$ $\rho_{\text{ave}} = 1.08 \times 10^{12} / \text{m}^2$

<u>Foil No.</u>	<u>Micrograph No.</u>	<u>Magnification</u>	<u>Dislocations</u>
A-3, 12	8423	20,000x	30
A-3, 12	8424	20,000x	10
A-3, 12	8425	20,000x	17
A-3, 12	8426	20,000x	13
A-3, 12	8427	20,000x	19
A-3, 12	8428	20,000x	25
A-3, 12	8429	20,000x	30
A-3, 12	8430	20,000x	42
A-3, 12	8431	20,000x	19
A-3, 12	8432	20,000x	48
A-3, 12	8433	20,000x	20
A-3, 12	8434	20,000x	4
A-3, 12	8435	20,000x	23
A-3, 12	8436	20,000x	35
A-3, 12	8437	20,000x	33
A-3, 13	8415	20,000x	1
A-3, 13	8416	20,000x	9
A-3, 13	8417	20,000x	13
A-3, 13	8418	20,000x	2
A-3, 13	8419	20,000x	3
A-3, 13	8420	20,000x	3
A-3, 13	8421	20,000x	6
A-3, 13	8422	20,000x	6

TABLE B.3

Specimen A-4, $\epsilon = 1.26$, $\dot{\epsilon} = 5.04 \times 10^{-4} \text{ s}^{-1}$ $T = 644 \text{ K}$, $\lambda_{\text{ave}} = 12.60 \text{ } \mu\text{m}$ $\rho_{\text{ave}} = 2.08 \times 10^{12} / \text{m}^2$

<u>Foil No.</u>	<u>Micrograph No.</u>	<u>Magnification</u>	<u>Dislocations</u>
A-4,7	8404	20,000x	36
A-4,7	8405	20,000x	2
A-4,7	8406	20,000x	17
A-4,7	8407	20,000x	37
A-4,7	8408	20,000x	36
A-4,7	8409	20,000x	44
A-4,7	8410	20,000x	9
A-4,7	8411	20,000x	49
A-4,7	8412	20,000x	22
A-4,7	8413	20,000x	32
A-4,8	8395	20,000x	33
A-4,8	8396	20,000x	51
A-4,8	8397	20,000x	39
A-4,8	8398	20,000x	47
A-4,8	8399	20,000x	51
A-4,8	8400	20,000x	36
A-4,8	8401	20,000x	33
A-4,8	8402	20,000x	26
A-4,8	8403	20,000x	54

TABLE B.4

Specimen A-5, $\varepsilon = 4.05$, $\dot{\varepsilon} = 5.04 \times 10^{-4} \text{ s}^{-1}$ $T = 644 \text{ K}$, $\lambda_{\text{ave}} = 12.30 \text{ } \mu\text{m}$ $\rho_{\text{ave}} = 1.09 \times 10^{12} / \text{m}^2$

<u>Foil No.</u>	<u>Micrograph No.</u>	<u>Magnification</u>	<u>Dislocations</u>
A-5,6	7391	20,000x	8
A-5,6	7392	20,000x	6
A-5,6	7393	20,000x	12
A-5,6	7394	20,000x	7
A-5,6	7395	20,000x	19
A-5,6	7396	20,000x	12
A-5,6	7400	20,000x	3
A-5,6	7401	20,000x	14
A-5,6	7402	20,000x	8
A-5,6	7403	20,000x	1
A-5,6	7404	20,000x	15
A-5,6	7405	20,000x	1
A-5,6	7406	20,000x	3
A-5,6	7407	20,000x	6
A-5,9	7412	20,000x	19
A-5,9	7413	20,000x	17
A-5,9	7414	20,000x	26
A-5,9	7415	20,000x	28
A-5,9	7416	20,000x	44
A-5,9	7417	20,000x	13
A-5,9	7418	20,000x	23
A-5,9	7419	20,000x	46
A-5,9	7420	20,000x	38
A-5,9	7421	20,000x	42
A-5,9	7422	20,000x	38

TABLE B.5

Specimen A-6, $\varepsilon = 0.10$, $\dot{\varepsilon} = 5.04 \times 10^{-4} \text{ s}^{-1}$ $T = 644 \text{ K}$, $\lambda_{\text{ave}} = 15.35 \text{ } \mu\text{m}$ $\rho_{\text{ave}} = 1.32 \times 10^{12} / \text{m}^2$

<u>Foil No.</u>	<u>Micrograph No.</u>	<u>Magnification</u>	<u>Dislocations</u>
A-6,8	7886	20,000x	2
A-6,8	7887	20,000x	12
A-6,8	7888	20,000x	6
A-6,8	7889	20,000x	23
A-6,8	7890	20,000x	48
A-6,8	7891	20,000x	16
A-6,8	7892	20,000x	33
A-6,8	7893	20,000x	30
A-6,8	7894	20,000x	54
A-6,8	7895	20,000x	26
A-6,8	7896	20,000x	36
A-6,8	7897	20,000x	27
A-6,8	7898	20,000x	49
A-6,8	7899	20,000x	36
A-6,8	7900	20,000x	14
A-6,8	7901	20,000x	10
A-6,8	7902	20,000x	4
A-6,8	7903	20,000x	28
A-6,8	7904	20,000x	30
A-6,8	7905	20,000x	14

TABLE B:5 (CONTINUED)

<u>Foil No.</u>	<u>Micrograph No.</u>	<u>Magnification</u>	<u>Dislocations</u>
A-6,13	7858	20,000x	18
A-6,13	7859	20,000x	10
A-6,13	7860	20,000x	20
A-6,13	7861	20,000x	22
A-6,13	7862	20,000x	10
A-6,13	7863	20,000x	36
A-6,13	7864	20,000x	16
A-6,13	7865	20,000x	20
A-6,13	7866	20,000x	8
A-6,13	7867	20,000x	14
A-6,13	7868	20,000x	6
A-6,13	7869	20,000x	7
A-6,13	7870	20,000x	20
A-6,13	7871	20,000x	14
A-6,13	7872	20,000x	14
A-6,13	7873	20,000x	22
A-6,13	7874	20,000x	24
A-6,13	7875	20,000x	30
A-6,13	7876	20,000x	25
A-6,13	7877	20,000x	26
A-6,13	7878	20,000x	42
A-6,13	7879	20,000x	30
A-6,13	7880	20,000x	16
A-6,13	7881	20,000x	9

TABLE B.6

Specimen A-7, $\epsilon = 7.89$, $\dot{\epsilon} = 5.04 \times 10^{-4} \text{ s}^{-1}$ $T = 644 \text{ K}$, $\lambda_{\text{ave}} = 15.92 \text{ } \mu\text{m}$ $\rho_{\text{ave}} = 4.24 \times 10^{12} / \text{m}^2$

<u>Foil No.</u>	<u>Micrograph No.</u>	<u>Magnification</u>	<u>Dislocations</u>
A-7,10	7906	20,000x	92
A-7,10	7907	20,000x	126
A-7,10	7908	20,000x	100
A-7,10	7909	20,000x	76
A-7,10	7910	20,000x	66
A-7,10	7911	20,000x	46
A-7,10	7912	20,000x	48
A-7,10	7913	20,000x	43
A-7,10	7914	20,000x	43
A-7,10	7915	20,000x	45
A-7,10	7916	20,000x	86
A-7,10	7917	20,000x	68
A-7,10	7918	20,000x	70
A-7,10	7919	20,000x	105
A-7,10	7420	20,000x	58
A-7,10	7421	20,000x	63
A-7,10	7422	20,000x	73
A-7,10	7423	20,000x	43
A-7,10	7424	20,000x	85
A-7,10	7426	20,000x	83
A-7,10	7427	20,000x	66
A-7,10	7428	20,000x	73
A-7,10	7429	20,000x	54

TABLE B.7

Specimen A-8, $\epsilon = 14.3$, $\dot{\epsilon} = 5.04 \times 10^{-4} \text{ s}^{-1}$ $T = 644 \text{ K}$, $\lambda_{\text{ave}} = 10.98 \text{ } \mu\text{m}$ $\rho_{\text{ave}} = 1.82 \times 10^{12} / \text{m}^2$

<u>Foil No.</u>	<u>Micrograph No.</u>	<u>Magnification</u>	<u>Dislocations</u>
A-8,2	7930	20,000x	32
A-8,2	7931	20,000x	31
A-8,2	7932	20,000x	24
A-8,2	7933	20,000x	14
A-8,2	7934	20,000x	33
A-8,2	7935	20,000x	28
A-8,2	7936	20,000x	27
A-8,2	7937	20,000x	88
A-8,2	7938	20,000x	28
A-8,2	7939	20,000x	38
A-8,2	7940	20,000x	31
A-8,2	7941	20,000x	27
A-8,2	7942	20,000x	31
A-8,2	7943	20,000x	29
A-8,2	7444	20,000x	24
A-8,2	7445	20,000x	43
A-8,2	7446	20,000x	15
A-8,2	7447	20,000x	42
A-8,2	7448	20,000x	26
A-8,2	7449	20,000x	18
A-8,2	7450	20,000x	32
A-8,2	7451	20,000x	23
A-8,2	7452	20,000x	11
A-8,2	7453	20,000x	25

TABLE B.8

Specimen A-9, $\varepsilon = 16.3$, $\dot{\varepsilon} = 5.04 \times 10^{-4} \text{ s}^{-1}$ $T = 644 \text{ K}$, $\lambda_{\text{ave}} = 13.47 \text{ } \mu\text{m}$ $\rho_{\text{ave}} = 2.30 \times 10^{12} / \text{m}^2$

<u>Foil No.</u>	<u>Micrograph No.</u>	<u>Magnification</u>	<u>Dislocations</u>
A-9,2	7954	20,000x	60
A-9,2	7955	20,000x	20
A-9,2	7956	20,000x	86
A-9,2	7957	20,000x	46
A-9,2	7958	20,000x	38
A-9,2	7959	20,000x	47
A-9,2	7960	20,000x	35
A-9,2	7961	20,000x	31
A-9,2	7962	20,000x	43
A-9,2	7963	20,000x	57
A-9,2	7964	20,000x	27
A-9,2	7965	20,000x	36
A-9,2	7966	20,000x	22
A-9,2	7967	20,000x	27
A-9,2	7968	20,000x	42
A-9,2	7969	20,000x	34
A-9,2	7970	20,000x	52
A-9,2	7971	20,000x	22
A-9,2	7972	20,000x	14
A-9,2	7973	20,000x	40
A-9,2	7974	20,000x	39
A-9,2	7975	20,000x	41
A-9,2	7976	20,000x	23
A-9,2	7977	20,000x	39

TABLE B.8 (CONTINUED)

<u>Foil No.</u>	<u>Micrograph No.</u>	<u>Magnification</u>	<u>Dislocations</u>
A-9,7	8895	20,000x	8
A-9,7	8896	20,000x	15
A-9,7	8897	20,000x	12
A-9,7	8898	20,000x	6
A-9,7	8899	20,000x	17
A-9,7	8900	20,000x	11
A-9,7	8901	20,000x	32
A-9,7	8902	20,000x	16
A-9,7	8903	20,000x	5
A-9,7	8904	20,000x	10
A-9,7	8905	20,000x	23

TABLE B.9

Specimen A-11, $\epsilon = 6.33$, $\dot{\epsilon} = 5.04 \times 10^{-4} \text{ s}^{-1}$ $T = 644 \text{ K}$, $\lambda_{\text{ave}} = 13.73 \text{ } \mu\text{m}$ $\rho_{\text{ave}} = 1.34 \times 10^{12} / \text{m}^2$

<u>Foil No.</u>	<u>Micrograph No.</u>	<u>Magnification</u>	<u>Dislocations</u>
A-11,3	8748	20,000x	24
A-11,3	8749	20,000x	24
A-11,3	8750	20,000x	21
A-11,3	8751	20,000x	9
A-11,3	8752	20,000x	6
A-11,3	8753	20,000x	13
A-11,3	8754	20,000x	5
A-11,3	8755	20,000x	12
A-11,3	8756	20,000x	15
A-11,3	8757	20,000x	14
A-11,3	8758	20,000x	19
A-11,3	8759	20,000x	18
A-11,4	8772	20,000x	16
A-11,4	8773	20,000x	25
A-11,4	8774	20,000x	22
A-11,4	8775	20,000x	22
A-11,4	8776	20,000x	39
A-11,4	8777	20,000x	42
A-11,4	8778	20,000x	36
A-11,4	8779	20,000x	20
A-11,4	8780	20,000x	36
A-11,4	8781	20,000x	18
A-11,4	8782	20,000x	48
A-11,4	8783	20,000x	28

TABLE B.10

Specimen A-12, $\varepsilon = 0.20$, $\dot{\varepsilon} = 5.04 \times 10^{-4} \text{ s}^{-1}$ $T = 644 \text{ K}$, $\lambda_{\text{ave}} = 11.27 \text{ } \mu\text{m}$ $\rho_{\text{ave}} = 1.12 \times 10^{12} / \text{m}^2$

<u>Foil No.</u>	<u>Micrograph No.</u>	<u>Magnification</u>	<u>Dislocations</u>
A-12,2	8567	20,000x	9
A-12,2	8568	20,000x	14
A-12,2	8569	20,000x	21
A-12,2	8570	20,000x	3
A-12,2	8571	20,000x	30
A-12,2	8572	20,000x	11
A-12,2	8573	20,000x	3
A-12,2	8574	20,000x	11
A-12,2	8575	20,000x	9
A-12,2	8576	20,000x	31
A-12,2	8577	20,000x	17
A-12,2	8578	20,000x	10
A-12,2	8579	20,000x	19
A-12,2	8580	20,000x	36
A-12,2	8581	20,000x	32
A-12,2	8582	20,000x	18
A-12,2	8583	20,000x	22
A-12,2	8584	20,000x	20
A-12,2	8585	20,000x	33
A-12,2	8586	20,000x	21

TABLE B.11

Specimen A-13, $\epsilon = 0.03$, $\dot{\epsilon} = 5.04 \times 10^{-4} \text{ s}^{-1}$ $T = 644 \text{ K}$, $\lambda_{\text{ave}} = 44.07 \text{ } \mu\text{m}$ $\rho_{\text{ave}} = 1.03 \times 10^{12} / \text{m}^2$

<u>Foil No.</u>	<u>Micrograph No.</u>	<u>Magnification</u>	<u>Dislocations</u>
A-13,2	8531	20,000x	23
A-13,2	8532	20,000x	17
A-13,2	8533	20,000x	5
A-13,2	8534	20,000x	24
A-13,2	8535	20,000x	10
A-13,2	8536	20,000x	10
A-13,2	8537	20,000x	3
A-13,2	8538	20,000x	20
A-13,2	8539	20,000x	21
A-13,2	8540	20,000x	32
A-13,3	8546	20,000x	20
A-13,3	8547	20,000x	10
A-13,3	8548	20,000x	23
A-13,3	8549	20,000x	21

LIST OF REFERENCES

1. Mieszczański, P. P., *The Variation in the Subgrain Size in Aluminum Deformed to Large Steady-State Creep Strains*, M.S. Thesis, Naval Postgraduate School, Monterey, California, September 1985.
2. Ferreira, I., and Stang, R. G., "The Effect of Stress and Subgrain Size on the Creep Behavior of High Purity Aluminum," *Acta Metallurgica*, Vol. 31, p. 585, 1983.
3. Soliman, M. S., Ginter, T. J., and Mohamed, F. A., "An Investigation of the Stress Exponent and Subgrain Size in Al After Stress Reduction," *Philosophical Magazine A*, Vol. 48, No. 1, p.73, 1983.
4. Kikuchi, S. and Yamaguchi, A., "Effects of Prestrain at High Temperatures on the Strength of Aluminum," *Strength of Metals and Alloys*, H. J. McQueen, et al., ed., Pergamon Press, Oxford, p. 899, 1985.
5. Young, C. M., Robinson, S. L., and Sherby, O. D., "Effect of Subgrain Size on the High Temperature Strength of Polycrystalline Aluminum as Determined by Constant Strain Rate Tests," *Acta Metallurgica*, Vol. 23, p. 633, May 1975.
6. Calliard and Martin, "Microstructure of Aluminum During Creep at Intermediate Temperature-II, In Situ Study of Subboundary Properties," *Acta Metallurgica*, Vol. 30, p. 791, 1982.
7. Langdon, T. G., Vastava, R. B., and Yavari, P., *Strength of Metals and Alloys*, P. Hassen, V. Gerold and G. Kostorz, eds., Pergamon Press, Oxford, p. 271, 1979.
8. Parker, J. D., and Wilshire, B., "On the Subgrain Size Dependence of Creep," *Philosophical Magazine A*, Vol. 34, p. 485, 1976.

9. Kassner, M. E., Ziaai-Moayyed, A. A., and Miller, A. K., "Some Trends Observed in the Elevated-Temperature Kinematic and Isotropic Hardening of Type 304 Stainless Steel," *Metallurgical Transactions A*, Vol. 16A, p. 1069, 1985.
10. Kassner, M. E., and Elmer, J. W., "Variations in the Spacing of Dislocations in Subgrain Boundaries with Creep Strain in Type 304 Stainless Steel," *Strength of Materials and Alloys*, H. J. McQueen, et al., ed., Pergamon Press, Oxford, p. 953, 1985.
11. Kassner, M. E., and Echer, C. J., "Mechanical Damage Introduced into Aluminum Monocrystals during TEM Thin-foil Preparation", *Metallography*, Vol. 19, p. 127, 1986.
12. Orlova, A., Tobolova, Z. and Cadek, J., "Internal Stress and Dislocation Structure of Aluminum in High-Temperature Creep", *Philosophical Magazine A*, Vol. 26, p. 1263, Dec. 1972.
13. Hirsch, Howie, Nicholson, Pashley and Whelan, *Electron Microscopy of Thin Crystals*, Butterworths, London, 1969.
14. Blum, W., Absenger, A. and Feilhauer, R., "Dislocation Structure in Al-Zn During Transient and Steady-State Creep," *Strength of Metals and Alloys*, Hansen, P., Gerold, V. and Kostorz, G., eds., Pergamon Press, Oxford, pp. 265-271, 1979.
15. Morris, M. A. and Martin, J. L., "Evolution of Internal Stresses and Substructure During Creep at Elevated Temperature," *Acta Metallurgica*, Vol. 32, p. 549, 1984.
16. Mitra, S. K. and McLean, D., "Cold Work and Recovery at Ostensibly Constant Structure," *Journal of Materials Science*, Vol. 1, p. 192, 1967.
17. Ostrom, P. and Lagneborg, R., "A Dislocation Link-Length Model for Creep," *Res Mechanica*, Vol. 1, p. 59, 1980.
18. Ardell, A. J. and Przystupa, M. A., "Dislocation Link-Length Statistics and Elevated Temperature Deformation of Crystals," *Mechanics of Materials*, Vol. 3, p. 319, 1984.

INITIAL DISTRIBUTION LIST

	No.	Copies
1. Library, Code 0142 Naval Postgraduate School Monterey, California 93943-5002	2	
2. Department Chairman, Code 69Mx Department of Mechanical Engineering Naval Postgraduate School Monterey, California 93943-5000	1	
3. Professor M. E. Kassner, Code 69 Department of Mechanical Engineering Naval Postgraduate School Monterey, California 93943-5000	5	
4. Commanding Officer, Code 330 Attn: LT T. S. Wetter Yokosuka Naval Ship Repair Facility Yokosuka, Honshu, Japan	1	
5. Defence Technical Information Center Cameron Station Alexandria, Virginia 22304-6145	2	